Biochimie 107 (2014) 396–405

Contents lists available at ScienceDirect

Biochimie

journal homepage: www.elsevier.com/locate/biochi

Research paper

Mutational analysis of residues in human arsenic (III) methyltransferase (hAS3MT) belonging to 5 Å around S-adenosylmethionine (SAM)

Xiangli Li [a], Zhirong Geng [a, *], Jiayin Chang [a], Xiaoli Song [b], Zhilin Wang [a, *]

[a] State Key Laboratory of Coordination Chemistry, School of Chemistry and Chemical Engineering, Nanjing University, Nanjing 210093, PR China
[b] School of Chemistry and Chemical Engineering, Yangzhou University, Yangzhou 225002, PR China

ARTICLE INFO

Article history:
Received 19 September 2014
Accepted 17 October 2014
Available online 25 October 2014

Keywords:
Human arsenic (III) methyltransferase (hAS3MT)
Mutants
S-adenosylmethionine (SAM)
SAM-binding sites

ABSTRACT

The functions of residues 57-RY-58, G60, L77, 80-GSGR-83, I101, T104, 134-GY-135, N155, V157 and 160-LV-161 in human arsenic (III) methyltransferase (hAS3MT) 5 Å around S-adenosylmethionine (SAM) have not been studied. Herein, sixteen mutants were designed by substituting these residues with Ala. Mutants G60A, G80A, I101A, N155A and L160A were completely inactive. Only MMA was detected when mutants R57A, Y58A, G82A and T104A were used as the enzymes, which suggested that their catalytic activities were seriously impaired compared with that of wild type (WT). The catalytic capacities of other mutants were also lower than that of WT-hAS3MT. The $K_{M(SAM)}$ values of mutants were 1.9–8.7 times that of WT, suggesting their affinities to SAM were weakened. As evidenced by the experimental data herein, earlier literature and the model of hAS3MT-SAM, 57-RYYG-60, G78, G80, G82 and 155-NCV-157 interacted with the methionine of SAM, and 101-IDMT-104 and 135-YIE-137 were associated with the nucleotide adenosine of SAM. Since C156 and L160 were the common residues between 5 Å around SAM and 5 Å around As, and C156S and L160A were inactive, we proposed that C156 and L160 functioned in the methyl transfer process. G78, G80 and G82 belonging to the consensus GxGxG were located in a loop connecting the first β-strand and α-helix in the Rossmann fold core. Y59, N155, C156 and L160 oriented S^{+}-CH_3 during its approach to the arsenic lone pair, and further activated methyl transfer. G78, D102, M103, T104, I136 and N155 formed hydrogen bonds with SAM.

1. Introduction

Arsenic has dual roles, one being potent toxin and carcinogens threatening human health, and the other being drugs against cancers such as acute promyelocytic leukemia [1–5]. Both of them are closely related with the metabolism of arsenic. Studying the mechanism of arsenic metabolism is crucial to relieve the toxicity of arsenic and to better exert its drug function. Arsenic (III) methyltransferase (AS3MT) is a main enzyme catalyzing the arsenic methylation which is a primary pathway of its metabolism, although N-6 adenine-specific DNA methyltransferase 1 also catalyzes some of MMA^{III} methylation [6–8]. AS3MT with reductant and methyl donor S-adenosylmethionine (SAM) catalyzes arsenic methylation [7,9,10], the mechanism of which has been studied for many years [11,12]. SAM binding to AS3MT is prerequisite for the methylation of substrate inorganic arsenic (iAs). It has been proposed that during methylation, SAM first binds AS3MT and then iAs binds it as the second substrate [13,14].

Active sites and As-binding sites of AS3MT have been studied. Residues C157 and C207 in recombinant mouse AS3MT, C156 in rat AS3MT, C61, C156 and C206 in human AS3MT (hAS3MT) and C72, C174 and C224 in *Cyanidioschyzon merolae* arsenite S-adenosylmethyltransferase (CmArsM) have been proved as their As-binding sites and active sites [15–19]. hAS3MT belongs to the Rossmann fold SAM-dependent methyltransferase, with highly conserved glycine-rich sequence of GxGxG as the hallmark

Abbreviations: iAs, inorganic arsenic; MMA, monomethylated arsenicals; DMA, dimethylated arsenicals; AS3MT, arsenic (III) methyltransferase; SAM, S-adenosylmethionine; IPTG, isopropyl β-D-thiogalactopyranoside; ATR-FTIR, attenuated total reflection Fourier transform infrared spectrometry; WT, wild-type; HPLC-ICP-MS, high performance liquid chromatography-inductively coupled plasma-mass spectrometry; SDS-PAGE, sodium dodecyl sulfate-polyacrylamide gel electrophoresis; CmArsM, cyanidioschyzon merolae arsenite S-adenosylmethyltransferase.

* Corresponding authors. Tel.: +86 25 83686082; fax: +86 25 83317761.
E-mail addresses: gengzr@nju.edu.cn (Z. Geng), wangzl@nju.edu.cn (Z. Wang).

http://dx.doi.org/10.1016/j.biochi.2014.10.014
0300-9084/

[7,20,21]. The predicted SAM-binding motifs of hAS3MT obtained via sequence alignment of various SAM-dependent methyltransferases are motif I 74-ILDLGSGSG-82, motif II 101-IDMT-104, motif III 147-ESHDIVVSN-155 and motif IV174-VLKHGGELYF-183 [6,7,20]. Parts of the functions of residues have been investigated [17,20,22]. The model of wild type (WT) hAS3MT with SAM shows that the residues belonging to 5 Å around SAM are 57-RYYG-60, 76-DLGSGSGRD-84, 101-IDMT-104, Q107, 134-GYIE-137, 155-NCV-157, 160-LV-161 and C206 [20,22]. Among them, the functions of residues Y59, D76, G78, S79, D84, D102, M103, Q107, I136, E137, C156 and C206 have been studied [17,20,22]. Mutants Y59A, D76N, G78A, D84N, D102N, C156S and C206S are completely inactive and the catalytic activities of mutants M103A, Q107A, I136A and E137A are lower than that of WT. The functions of the rest remain unknown hitherto.

To analyze the functions of overall residues located 5 Å around SAM and to determine the residues closely associated with SAM-binding, the functions of the remaining residues were evaluated. Sixteen mutants R57A, Y58A, G60A, L77A, G80A, S81A, G82A, R83A, I101A, T104A, G134A, Y135A, N155A, V157A, L160A and V161A were obtained by site-directed mutagenesis. Then, their catalytic activities and secondary conformation were gauged, and models of mutants with SAM were also built and analyzed. Mutants G60A, G80A, I101A, N155A and L160A were completely deprived of catalytic activities. Only MMA was produced when mutants R57A, Y58A, G82A and T104A were used as the enzymes, suggesting their catalytic activities were seriously weakened. The catalytic capacities of L77A, S81A, R83A, G134A, Y135A, V157A and V161A were also decreased. As indicated by the experimental data in this study, earlier literature and hAS3MT-SAM model, residues 57-RYYG-60, 76-DLGSGSGRD-84, 101-IDMT-104, 134-GYIE-137, 155-NCV-157, 160-LV-161 and C206 in hAS3MT synergistically formed the SAM-binding domain, especially the hydrophobic residues G60, L77, G78, G80, G82, I101, M103, G134, I136, V157, L160 and V161, the aromatic residues Y58 and Y59, and the polar with charge residues R57, D76, R83, D84, D102, E137, N155, C156 and C206. 57-RYYG-60, 78-GSGSG-82 and 155-NC-157 interacted with methionine of SAM. Meanwhile, 101-IDMT-103 and 135-YIE-137 closely contacted with nucleotide adenosine of SAM. C156 and L160, as common residues between 5 Å around SAM and 5 Å around As, functioned in the methyl transfer process. G78, G80 and G82 belonging to the consensus GxGxG were located in a loop connecting the first β-strand and α-helix in the Rossmann fold core. Y59, N155, C156 and L160 interacting with S^{+}-CH_3 of SAM assisted to orient S^{+}-CH_3 during its approach to the arsenic lone pair and further activated methyl transfer. G78, D102, M103, T104, I136 and N155 formed hydrogen bonds with SAM.

2. Materials and methods

Caution: Arsenic has been known as a carcinogen and should be handled carefully [23].

2.1. Materials

SAM, GSH, isopropyl β-D-thiogalactopyranoside (IPTG) and bovine serum albumin (BSA) were purchased from Sigma. Arsenicals were bought from J&K Chemical Ltd. Phosphate-buffered saline (PBS, pH 7.0) buffer was prepared by mixing appropriate volumes of Na_2HPO_4 and NaH_2PO_4 into a 25 mM stock solution. $NaAsO_2$ (As^{3+}), $Na_2HAsO_4{\cdot}7H_2O$ (As^{5+}), disodium methylarsonate (MMA^{5+}) and dimethylarsinic acid (DMA^{5+}) were obtained from J&K Chemical Ltd.

2.2. Protein expression and purification

Sixteen mutants (R57A, Y58A, G60A, L77A, G80A, S81A, G82A, R83A, I101A, T104A, G134A, Y135A, N155A, V157A, L160A and V161A) and WT-hAS3MT were prepared as described previously [24]. The primers for site-directed mutagenesis are summarized in Table 1. Protein expression and purification were performed according to the protocols detailed in previous literature [17,24]. The method of Bradford based on a BSA standard curve was used to determine protein concentrations [25].

2.3. Determining the catalytic activity of the hAS3MT mutants

Solutions (100 μl) containing 11 μg enzyme, 7 mM GSH, 1 μM iAs^{3+} and 1 mM SAM in PBS (25 mM, pH 7.0) were incubated at 37 °C for 2 h, and then the reaction was terminated by adding H_2O_2 to a final concentration of 3%. Finally, the arsenic species were separated on an anion-exchange column by HPLC (PRP X-100 250 mm × 4.6 mm i.d., 5 μm, Hamilton) and analyzed by ICP-MS (Elan 9000, PerkinElmer) [26,27]. The arsenic species were eluted with 12 mM $(NH_4)_2HPO_4$ as the mobile phase, the pH of which was adjusted to 6.0 with H_3PO_4. To determine the iAs kinetic parameters, various iAs concentrations (0.5–500 μM) were used without changing other conditions. In the SAM kinetic experiments, 0.05–1 mM SAM were used. Working curve prepared using 5, 10, 25, 50 and 100 μg/L standard arsenic species was used to calculate the amounts of arsenic species obtained from the reaction. The methylation rates were calculated as mole equivalents of methyl groups that were transferred from SAM to iAs^{3+} (i.e., 1 pmol CH_3 per 1 pmol MMA or 2 pmol CH_3 per 1 pmol DMA) [28]. Noncompetitive substrate inhibition Eq. (1): $V = [S] * V_{max}/(K_M + [S] + [S]^2/$

Table 1
Primers used for site-directed mutagenesis.

	Primer	Sequence
R57A	+	5′-CGAAGAAGTAGCCCTA**GCG**TATTATG-3′
	−	5′−GCCATAATA**CGC**TAGGGCTACTTCTTCG-3′
Y58A	+	5′-CGAAGAAGTAGCCCTAAGA**GCG**TATGG-3′
	−	5′-AGACCACAGCCATA**CGC**TCTTAGGG-3′
G60A	+	5′-AGCCCTAAGATATTAT**GCG**TGTGG-3′
	−	5′-CAGACCACA**CGC**ATAATATCTTAGGGC-3′
L77A	+	5′-GCTGGATTTTGGAT**GCG**GGTAG-3′
	−	5′−TCCACTACC**CGC**ATCCAAAATCCAG-3′
G80A	+	5′-CTGGGTAGT**GCG**AGTGGTAGAGATTG-3′
	−	5′-GCAATCTCTACCACT**CGC**ACTACCC-3′
S81A	+	5′-CTGGGTAGTGGA**GCG**GGTAGAGATT-3′
	−	5′−GCAATCTCTACC**CGC**TCCACTACC-3′
G82A	+	5′-GT**GCG**AGAGATTGCTATGTACTTAGCC-3′
	−	5′-GGCTAAGTACATAGCAATCTCT**CGC**AC-3′
R83A	+	5′-GAAGTGGT**GCG**GATTGCTATGTA-3′
	−	5′-GGCTAAGTACATAGCAATC**CGC**ACC-3′
I101A	+	5′-AAAAGGACACGTGACTGGA**GCG**GAC-3′
	−	5′-TGGCCTTTGGTCATGTC**CGC**TCC-3′
T104A	+	5′-GACTGGAATAGACATG**GCG**AAAGGC-3′
	−	5′-TCCACCTGGCCTTT**CGC**CATGTCTA-3′
G134A	+	5′-GCATCTAATGTGACTTTTATTCAT**GCG**TAC-3′
	−	5′-TCTCCCAACTTCTCAATGTA**CGC**ATG-3′
Y135A	+	5′-GACTTTTATTCATGGC**GCG**ATTGAG-3′
	−	5′-ACTTCTCAAT**CGC**GCCATGAATAAA-3′
N155A	+	5′-GCCATGATATTGTTGTATCA**GCG**TGTG-3′
	−	5′-GGCACAAGGTTAATAACACA**CGC**TGATAC-3′
V157A	+	5′-TATTGTTGTATCAAACTGT**GCG**ATTAACC-3′
	−	5′-GGCACAAGGTTAAT**CGC**ACAGTTTGATAC-3′
L160A	+	5′-ACTGTGTTATTAAC**GCG**GTGCCTGA-3′
	−	5′-GTTTATCAGGCAC**CGC**GTTAATAACAC-3′
V161A	+	5′-CAAACTGTGTTATTAACCTT**GCG**CCTG-3′
	−	5′-GCACTTGTTGTTTATCAGG**CGC**AAG-3′
Whole	+	5′-CGGGATATCATGGCTGCACTTCGTGAC-3′
	−	5′-CGGGTCGACTTAGTGATGGTGATG-3′

K_I) and double reciprocal Eq. (2): $1/V = K_M/(V_{max} * [S]) + 1/V_{max}$ [17,29] were used to calculate the kinetic parameters, where V is the initial velocity of the reaction (pmol CH_3 transferred/h/mg protein), [S] is the substrate (iAs^{3+}) concentration (μM), V_{max} is the maximal velocity of the reaction (pmol CH_3 transferred/h/mg protein), K_M is the Michaelis constant for iAs^{3+} or SAM (μM), and K_I is the inhibition constant for iAs^{3+} (μM) [30].

2.4. Monitoring the conformational changes of hAS3MT mutants compared with WT

CD spectra of the WT and hAS3MT mutants (2 μM in 25 mM PBS, pH 7.0) were recorded between 190 and 265 nm using a JASCO-J810 spectropolarimeter (Jasco Co., Japan) as previously described [17,20,22]. The scanning rate was set at 50 nm/min. Each spectrum represents the average of three accumulations and baseline correction was automatically carried out with the PBS (25 mM, pH 7.0) spectrum throughout the entire collection. The secondary structure parameters of mutants were calculated using Jwsse32 software with reference CD-Yang. jwr [31]. ATR-FTIR spectra were applied to determine the secondary structures of mutants. More details about the ATR-FTIR spectra were addressed in previous literature [17,32,33].

2.5. Modeling the hAS3MT mutants with cofactor SAM

hAS3MT and CmArsM were arsenic methyltransferases in different species with similar sequences, so models of hAS3MT-SAM were built by modeller9v8 with the most updated protein template CmArsM (PDB code 4FR0) [34]. The model quality of hAS3MT mutants was estimated via QMEAN Server (http://swissmodel.expasy.org/qmean/cgi/index.cgi) [35]. Pymol was used to analyze the models of hAS3MT [36].

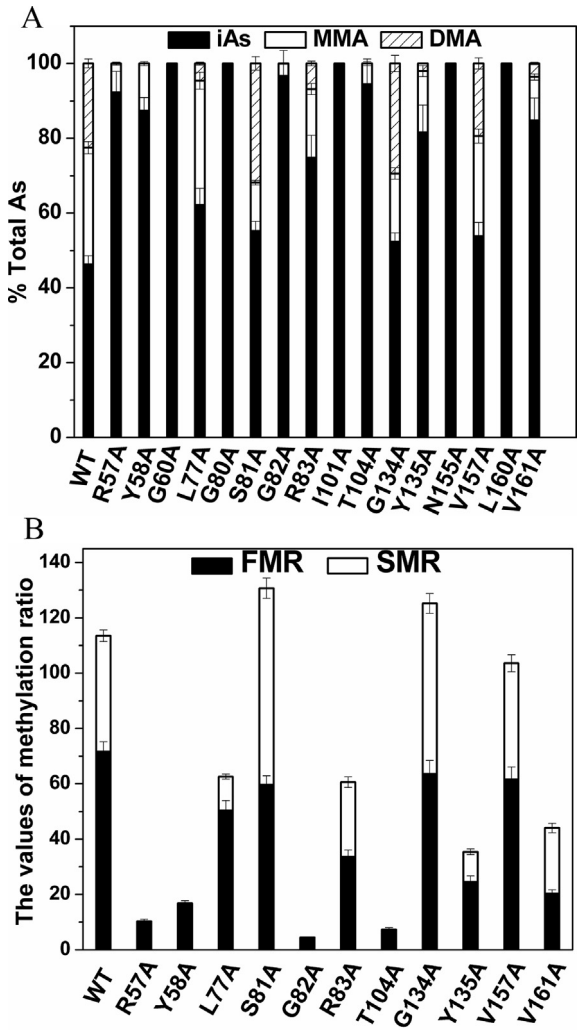

Fig. 1. Catalytic capacity of hAS3MT mutants. Reaction mixtures (100 μl) containing 11 μg enzymes, 1 μM iAs^{3+}, 1 mM SAM and 7 mM GSH in PBS (25 mM, pH 7.0) were incubated at 37 °C for 2 h with H_2O_2 treatment before being analyzed by HPLC-ICP-MS. The percents of arsenic species (iAs/TAs, MMA/TAs and DMA/TAs) and two indices (FMR and SMR) of mutants R57A, Y58A, L77A, G80A, S81A, R83A, T104A, G134A, Y135A, V157A and V161A are shown in A and B. Values are averages ± S.D. of three independent experiments performed by three independently purified proteins.

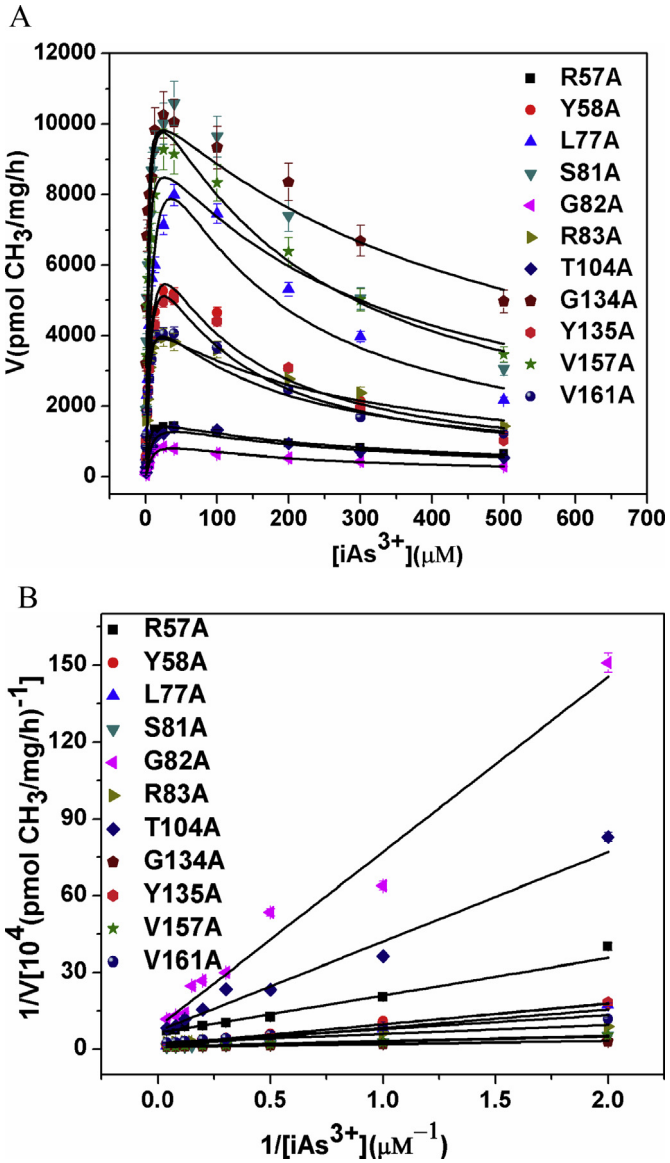

Fig. 2. A. Substrate concentration dependence of rate. The lines show the least squares fit of Eq. (1) to the data. B. Double reciprocal plots of the arsenic methylation rate against the concentration of iAs^{3+}. Reaction mixtures (100 μl) containing 11 μg enzymes, 1 mM SAM and 7 mM GSH in PBS (25 mM, pH 7.0) were incubated with different concentrations of iAs^{3+} at 37 °C for 2 h with H_2O_2 treatment before analysis. Values are averages ± S.D. of three independent experiments performed by three independently purified proteins.

Table 2
Kinetic parameters of arsenic methylation for eleven mutants R57A, Y58A, L77A, S81A, G82A, R83A, T104A, G134A, Y135A, V157A and V161A.

	[a]V_{max} (pmol CH_3/mg/h)	[a]K_M(μM)	K_I (mM)	[b]V_{max} (pmol CH_3/mg/h)	[b]K_M (μM)	[c]K_M (μM)	Relative [c]K_M
R57A	1686 ± 61	2.6 ± 0.2	0.29 ± 0.03	1586 ± 104	2.3 ± 0.4	349.1 ± 14.3	7.3
Y58A	8534 ± 748	7.6 ± 1.0	0.10 ± 0.02	6940 ± 783	5.7 ± 0.9	220.4 ± 15.2	4.6
L77A	12,153 ± 1244	9.6 ± 1.4	0.13 ± 0.03	12,996 ± 1167	7.0 ± 0.9	222.4 ± 13.6	4.6
S81A	11,979 ± 949	2.7 ± 0.5	0.21 ± 0.04	10,390 ± 933	2.1 ± 0.6	91.8 ± 7.5	1.9
G82A	1156 ± 162	8.7 ± 1.8	0.18 ± 0.05	1160 ± 96	7.9 ± 1.4	414.1 ± 20.3	8.7
R83A	4563 ± 196	1.8 ± 0.2	0.27 ± 0.03	4211 ± 178	1.5 ± 0.4	161.8 ± 8.4	3.4
T104A	1694 ± 204	7.0 ± 1.4	0.25 ± 0.07	1410 ± 159	4.9 ± 1.6	286.4 ± 9.8	6.0
G134A	10,819 ± 348	1.2 ± 0.1	0.48 ± 0.06	10,285 ± 665	1.1 ± 0.3	259.0 ± 11.3	5.4
Y135A	7936 ± 858	7.0 ± 1.2	0.09 ± 0.02	6144 ± 758	4.9 ± 1.8	156.2 ± 10.5	3.3
V157A	9938 ± 572	2.2 ± 0.3	0.31 ± 0.05	9113 ± 645	1.9 ± 0.5	142.0 ± 8.4	3.0
V161A	5084 ± 361	3.2 ± 0.5	0.17 ± 0.03	4361 ± 546	2.4 ± 0.6	329.6 ± 16.5	6.9
WT	21,170 ± 1079	3.2 ± 0.24	0.7 ± 0.09	19,836 ± 919	3.19 ± 0.7	47.8	1.0

Values represent average ± S.D. of three independent experiments performed by three independently purified proteins.
[a] Represents the kinetic parameters of iAs^{3+} estimated from the data in Fig. 2a by Eq. (1) using origin 8.0.
[b] Represents the kinetic parameters of iAs^{3+} calculated from the data in Fig. 2b.
[c] Represents the K_M for SAM.

3. Results

3.1. Catalytic activities of the hAS3MT mutants

Primary methylation rate (PMR) and secondary methylation rate (SMR) are defined as (MMA + DMA)/TAs and DMA/(MMA + DMA) respectively, in which TAs is the abbreviation of total arsenic [37]. In this study, however, TAs was the sum of iAs, MMA and DMA because trimethylated arsenic was not detected. Proportions of the arsenic species are defined as iAs/TAs, MMA/TAs and DMA/TAs [37]. The catalytic capacities of mutants were characterized by the proportions of the arsenic species, PMR and SMR (Fig. 1A and B). Fig. 1A shows that mutants G60A, G80A, I101A, N155A and L160A are completely deprived of their methylation capacities. Fig. 1A and B shows that mutants R57A, Y58A, G82A and T104A catalyze 3%–12% of iAs to MMA. Compared with WT-hAS3MT, the catalytic capacities of mutants L77A, R83A, Y135A and V161A are weakened (Fig. 1A and B). The catalytic capacities of mutants S81A, G134A and V157A are slightly lower than that of WT, while their SMR are higher than that of WT because more DMA is produced than MMA (Fig. 1A and B). Hence, residues G60, G80, I101, N155 and L160 as well as R57, Y58, G82 and T104 significantly affected the catalytic activity of hAS3MT.

To determine catalytic kinetic parameters, substrate iAs at wide-range concentrations were used. Methylation velocity presented an apparent first-order fashion at lower iAs concentrations, and then the reaction rate asymptotically approached the theoretical maximum (V_{max}) with increasing iAs concentration (0.5–40 μM) and finally decreased at higher iAs concentrations (100–500 μM). Plots of the inorganic arsenic concentrations versus the methylation rates fitted by Eq. (1) and the double reciprocal plots fitted by Eq. (2) for the mutants having methylation capacity are shown in Fig. 2A and B. The kinetic parameters calculated by Eq. (1) and Eq. (2) are summarized in Table 2. The V_{max} values of all mutants, especially those of R57A, G82A, R83A, T104A and V161A, are lower than that of WT, indicating their catalytic activities are weakened. The $K_{M(As)}$ values of mutants Y58A, L77A, G82A, T104A and Y135A are higher than that of WT, suggesting that their affinities to iAs are reduced.

3.2. Capacities of the mutants binding to SAM

The Michaelis constant for SAM, which is referred to as $K_{M(SAM)}$, is used as a relative measure of SAM binding affinity to hAS3MT

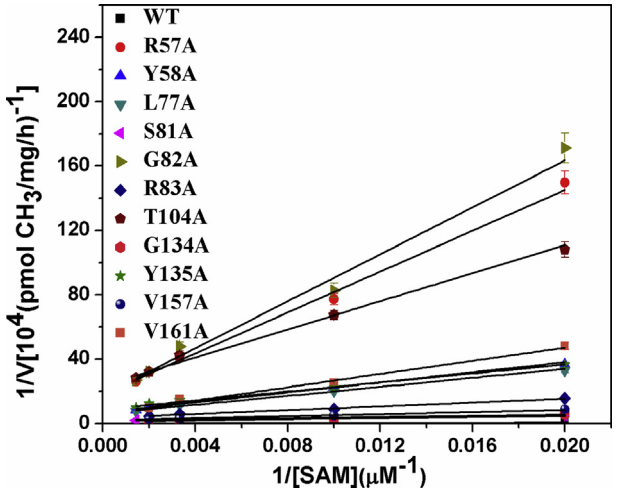

Fig. 3. Double reciprocal plots of the arsenic methylation rate versus the concentration of SAM. Reaction mixtures (100 μl) containing 11 μg enzymes, 1 μM iAs^{3+} and 7 mM GSH in PBS (25 mM, pH 7.0) were incubated with different concentrations of SAM for 2 h with H_2O_2 treatment before analysis. Values are averages ± S.D. of three independent experiments performed by three independently purified proteins.

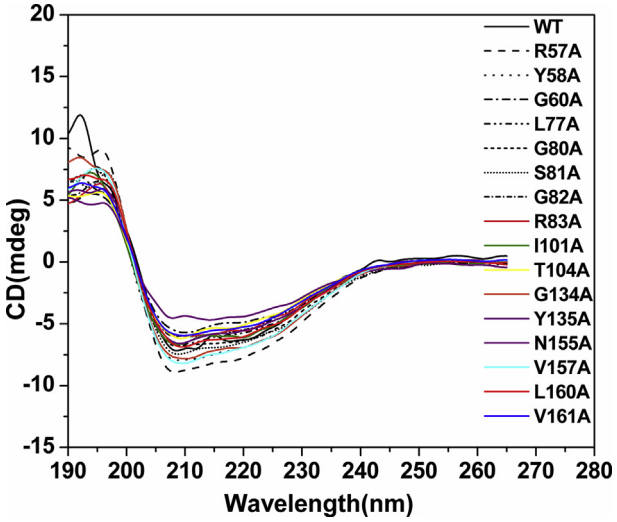

Fig. 4. CD spectra of hAS3MT and mutants. Spectra were taken at the protein concentration of 2 μM at room temperature. Plot is the representative of three independent measurements performed by three independently purified proteins.

[38]. The $K_{M(SAM)}$ values in Table 2 are calculated from the double reciprocal curves of methylation rates against SAM concentrations (Fig. 3). Since the $K_{M(SAM)}$ values of the mutants are 1.9–8.7 times that of WT, capacities of the mutants binding to SAM are weakened, which directly decrease their catalytic activities. Therefore, residues R57, Y58, L77, S81, G82, R83, T104, G134, Y135, V157 and V161 kept in close contact with SAM.

3.3. Conformations of the mutants characterized by CD and ATR-FTIR

CD spectroscopy sensitively determines the secondary structure of protein [39,40], which was employed to analyze the folding properties of the sixteen mutants (Fig. 4) to examine the effect of mutations on the folding and activity of enzyme. CD spectral intensities of mutants G60A, L77A, R83A, I101A, T104A, N155A, L160A and V161A are lower than that of WT, while the intensities of peaks at 208 nm and 220 nm of mutants R57A, Y58A, S81A, G134A and V157A exceed that of WT. Compared with WT, the peaks at 208 nm and 220 nm of N155A hypsochromically shift, suggesting that the conformation of N155A changes obviously. Thus, the conformations of the mutants are different from that of WT. The contents of secondary structures of the sixteen mutants were calculated by the Jwsse32 software with reference CD-Yang. jwr (Table 3a). The secondary structures of G60A, S81A, I101A, G134A and Y135A are similar to that of WT. Compared with WT, the contents of α-helix and β-turn in mutant N155A increase, while the content of β-pleated sheet decreases and that of random coil remains unchanged. For mutants R57A, G80A, L160A, and V161A, the contents of β-pleated sheet increase, whereas those of β-turn and random coil decrease, with the contents of α-helix barely changed. The contents of β-pleated sheet in mutants Y58A, L77A, G82A, R83A, T104A, and V157A increase with decreasing contents of α-helix, β-turn and random coil. Accordingly, the contents of secondary structures of mutants, except for those of G60A, S81A, I101A, G134A and Y135A, differed from those of WT.

Table 3
a. Secondary structures of WT-hAS3MT and mutants estimated from CD spectra. b. Secondary structures of WT-hAS3MT and mutants estimated from ATR-FTIR spectroscopy.

	α-helix%	β-pleated%	β-turn%	Random%
a)				
R57A	28.8 ± 2.3	28.0 ± 0.9*	15.2 ± 0.6	28.1 ± 1.2
Y58A	25.6 ± 1.1	31.3 ± 1.1**	14.3 ± 0.9*	28.8 ± 0.2
G60A	29.4 ± 1.6	24.3 ± 1.3	17.9 ± 0.8	28.4 ± 0.5
L77A	27.7 ± 0.3	28.6 ± 2.0*	14.5 ± 0.9*	29.2 ± 0.8
G80A	29.3 ± 1.2	26.1 ± 0.8	16.2 ± 1.0	28.4 ± 0.3
S81A	29.8 ± 2.4	22.8 ± 1.2	18.8 ± 0.6	28.6 ± 1.7
G82A	26.0 ± 1.6	33.0 ± 2.5**	13.3 ± 0.6*	27.8 ± 1.8
R83A	25.1 ± 1.2	34.2 ± 2.8**	13.4 ± 0.4*	27.3 ± 1.6
I101A	29.7 ± 1.4	25.0 ± 0.9	15.4 ± 0.6	29.8 ± 1.5
T104A	26.5 ± 1.7	31.5 ± 1.4**	14.4 ± 1.3*	27.6 ± 1.8
G134A	30.2 ± 2.2	25.3 ± 1.3	16.0 ± 1.0	28.5 ± 1.9
Y135A	29.6 ± 1.9	23.3 ± 1.0	18.6 ± 0.6	28.4 ± 1.6
N155A	32.6 ± 2.5	19.3 ± 0.8*	18.9 ± 0.8	29.2 ± 2.2
V157A	25.9 ± 1.4	31.1 ± 2.1*	15.4 ± 0.7	27.6 ± 1.5
L160A	29.8 ± 1.7	26.5 ± 1.5	16.2 ± 0.8	27.5 ± 1.7
V161A	29.2 ± 1.2	28.1 ± 1.4*	14.9 ± 0.6*	27.8 ± 1.3
WT	29.0 ± 2.2	23.9 ± 1.9	17.9 ± 1.7	29.2 ± 1.4
b)				
R57A	27.4 ± 2.3	29.0 ± 0.5*	12.3 ± 0.6**	31.2 ± 1.6
Y58A	28.4 ± 1.1	28.6 ± 1.1*	15.5 ± 1.0*	27.5 ± 0.8
G60A	28.3 ± 2.2	27.3 ± 2.0	18.2 ± 1.2*	26.2 ± 1.3
L77A	25.7 ± 1.0	28.5 ± 2.0	14.1 ± 0.5**	31.7 ± 0.6
G80A	28.3 ± 1.2	27.0 ± 0.8	18.2 ± 1.0*	26.5 ± 0.3
S81A	29.8 ± 3.2	23.9 ± 1.4	17.6 ± 1.4*	28.7 ± 2.5
G82A	27.8 ± 3.3	32.0 ± 3.5*	13.7 ± 0.8**	26.5 ± 2.3
R83A	26.9 ± 2.4	31.1 ± 2.8*	15.6 ± 1.0*	26.4 ± 1.4
I101A	29.7 ± 2.8	19.1 ± 1.4	21.4 ± 1.0	29.8 ± 3.3
T104A	26.3 ± 1.7	31.9 ± 1.4*	15.9 ± 1.3*	25.9 ± 1.8
G134A	30.8 ± 2.7	23.6 ± 1.3	17.9 ± 0.9*	27.7 ± 2.3
Y135A	30.6 ± 2.3	28.8 ± 1.6*	15.0 ± 0.9**	25.6 ± 1.7
N155A	31.0 ± 1.9	18.2 ± 0.8	21.1 ± 1.3	29.6 ± 2.6
V157A	26.5 ± 1.7	31.1 ± 2.6*	16.6 ± 1.0*	25.8 ± 1.6
L160A	32.1 ± 2.4	24.5 ± 1.2	16.5 ± 0.8*	26.9 ± 1.7
V161A	28.4 ± 2.5	30.8 ± 3.5*	15.2 ± 1.0**	25.5 ± 1.4
WT	26.6 ± 3.6	20.7 ± 4.6	24.2 ± 3.2	28.5 ± 4.9

Values represent average ± S.D. of three independent experiments carried out by three independently purified proteins. The parameters were analyzed with the Jasco secondary structure manager with the reference CD data-Yang. jwr in PBS (25 mM, pH 7.0) at room temperature. Compared to WT, $^{*}p < 0.05$, $^{**}p < 0.01$.

To further confirm the secondary structures of the mutants, we carried out ATR-FTIR assays and analyzed their amide I band spectra according to the well-established assignment criterion (1610–1640 cm^{-1}: β-pleated sheet, 1640–1650 cm^{-1}: random coil, 1650–1658 cm^{-1}: α-helix, and 1660–1700 cm^{-1}: β-turn) [41,42]. The original and curve-fitting FTIR spectra of mutants R57A, Y58A, G60A, G80A, S81A, G82A, R83A, I101A, T104A, Q107A, G134A, Y135A, N155A, V157A, L160A and V161A are shown in Fig. 5. There are six component bands in the amide I bands of the mutants. The contents of each secondary structure were calculated from the integrated areas of the component bands (Table 3b). The secondary structures of the mutants derived from ATR-FTIR, except for β-turn of R57A, α-helix and β-pleated of Y58A, β-pleated and β-turn of I101A, β-pleated of Y135A, and β-turn of WT, are basically consistent with those obtained from CD spectra. The differences between secondary structures derived from ATR-FTIR and those obtained from CD spectra for the same mutant may result from the two distinctly different methods [40,41].

3.4. SAM-binding sites of hAS3MT mutants R57A, Y58A, G60A, L77A, G80A, S81A, G82A, R83A, I101A, T104A, G134A, Y135A, N155A, V157A, L160A and V161A

Models of hAS3MT mutants were established with modeller9v8 by using the crystal structure of CmArsM with cofactor SAM (PDB code 4FR0) as the template. The model quality was estimated in the light of a QMEAN scoring function acceptably ranging between 0.60 and 0.65 [35]. The secondary structure arrangement of the hAS3MT model is almost identical to that of CmArsM [34]. The sites in the SAM-binding pocket (5.0 Å around SAM) of WT-hAS3MT and mutants (R57A, Y58A, G60A, L77A, G80A, S81A, G82A, R83A, I101A, T104A, G134A, Y135A, N155A, V157A, L160A and V161A) are displayed in Fig. 6 and Table 4. Compared with the model of WT-hAS3MT with SAM, Cys206 is not in the SAM-binding pocket of mutants G60A, G80A, S81A, G82A, T104A, G134A, V157A and V161A. Residue R83 is disconnected from mutants R57A, L77A, R83A, I101A, Y135A and N155A. The microenvironments of SAM for most mutants (except for L160A) vary from that of WT.

4. Discussion

SAM, which is a conjugate of nucleotide adenosine and amino acid methionine, provides diverse chemical groups for the biosynthesis and modification of important biomolecules [43]. One of the critical chemical groups provided by SAM, i.e. CH_3, is closely associated with the metabolism and modification of diverse molecules, such as lipids, proteins, DNA and other small molecules (inorganic arsenic, chloride, bromide) [44–46]. hAS3MT catalyzing arsenic methylation belongs to the Rossmann-fold SAM-dependent methyltransferase, with the highly conserved glycine-rich sequence of 74-ILDLGSGSG-82 as the hallmark. The SAM-binding sites in SAM-dependent methyltransferases have been deduced by sequences alignment [21]. Five highly conserved regions with

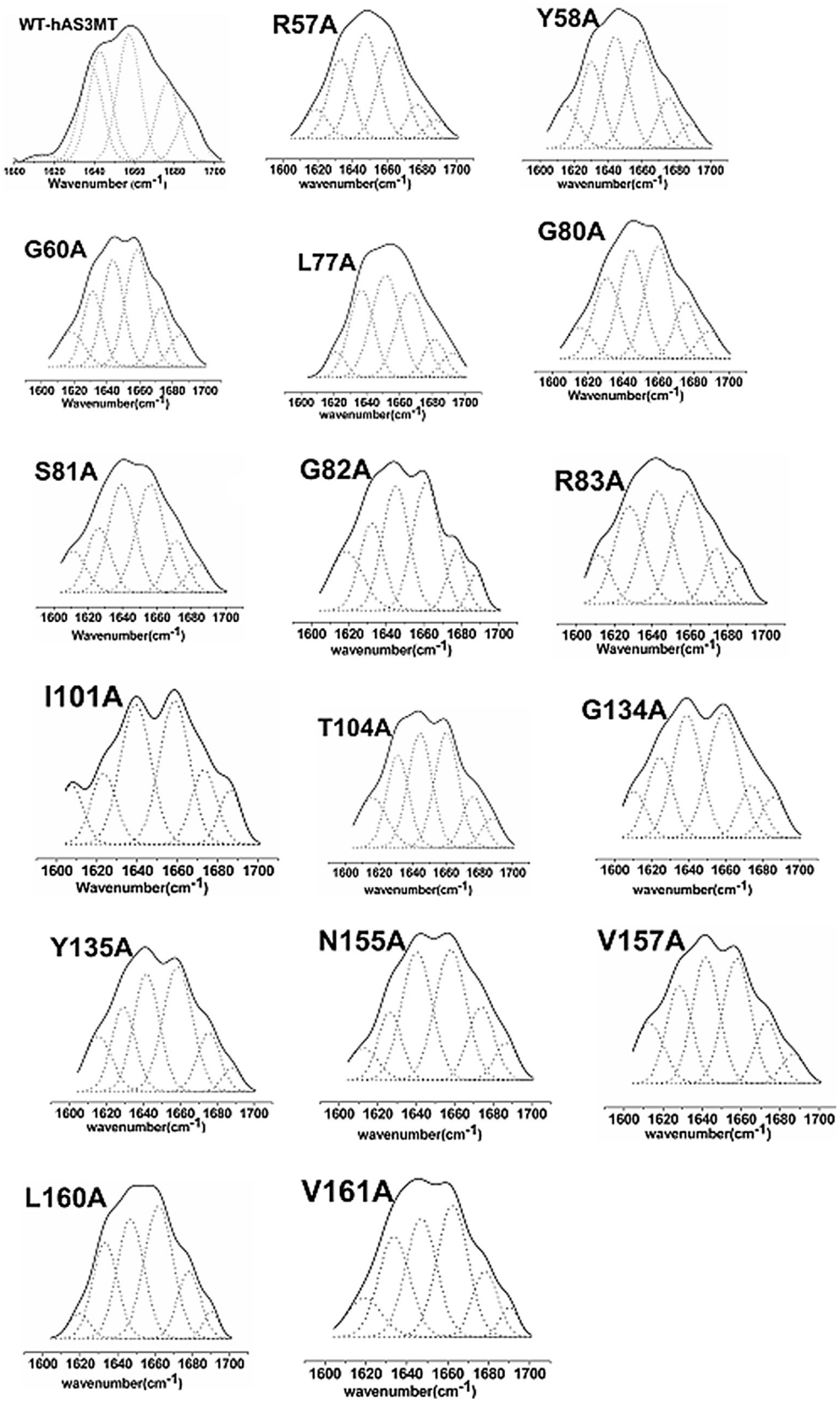

Fig. 5. Curve-fitted amide I region of WT-hAS3MT and mutants. The component peaks are the result of curve-fitting using a Gaussian shape. The solid lines represent the experimental FTIR spectra after Savitzky–Golay smoothing, and the dashed lines represent the fitted components. Plot is the representative of three independent measurements carried out by three independently purified proteins.

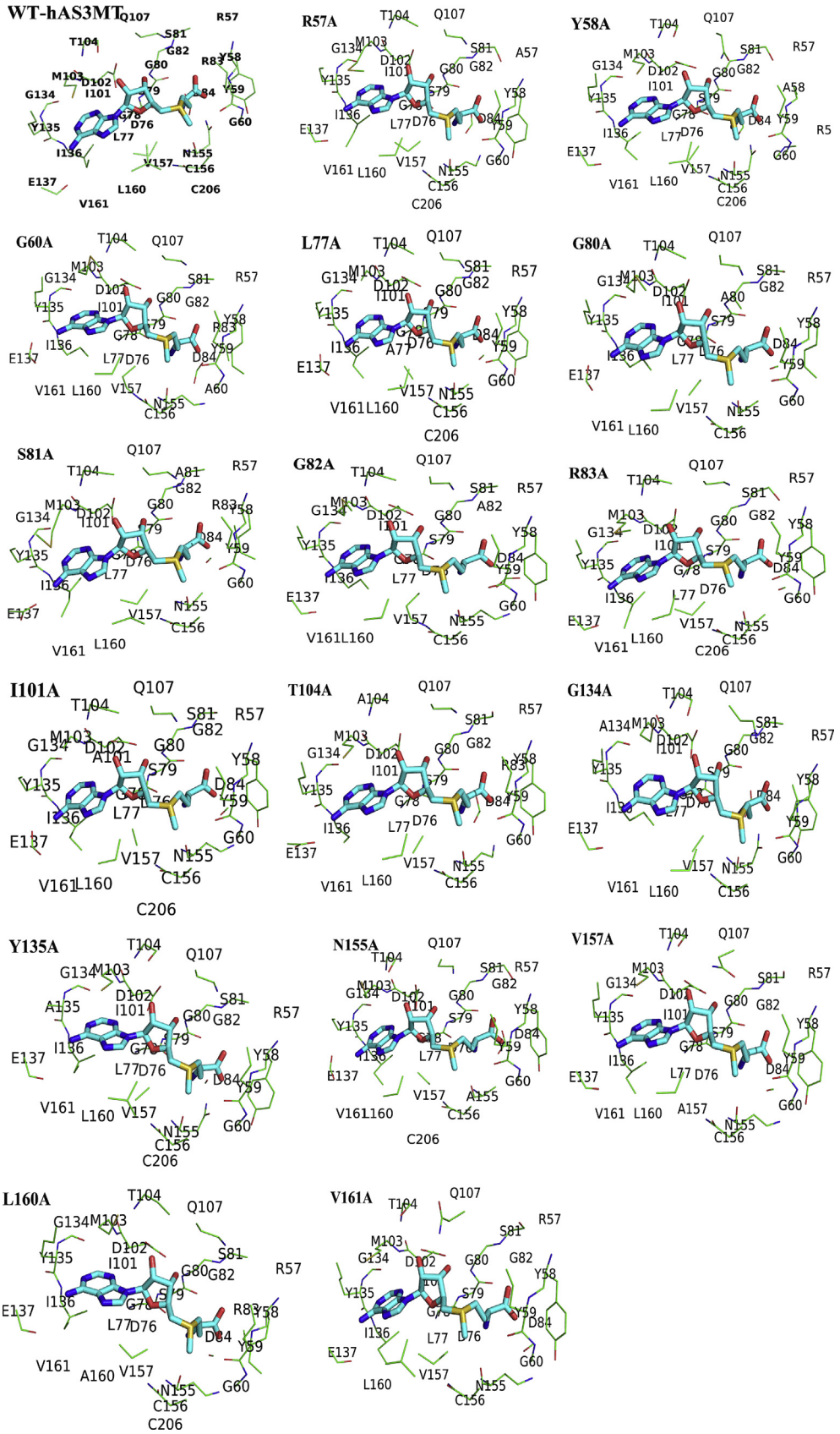

Fig. 6. Interaction modes between SAM, WT-hAS3MT and mutants (R57A, Y58A, G60A, L77A, G80A, S81A, G82A, R83A, I101A, T104A, G134A, Y135A, N155A, V157A, L160A and V161A). Only the residues 5.0 Å around SAM are displayed.

Table 4
Residues 5.0 Å around SAM based on the models of WT and mutants R57A, Y58A, G60A, L77A, G80A, S81A, G82A, R83A, I101A, T104A, G134A, Y135A, N155A, V157A, L160A and V161A.

	Residues 5.0 Å around SAM
WT	57-RYYG-60, 76-DLGSGSGRD-84, 101-IDMT-104, Q107, 134-GYIE-137, 155-NCV-157, 160-LV-161, C206
R57A	57-AYYG-60, 76-DLGSGSG-82, D84, 101-IDMT-104, Q107, 134-GYIE-137, 155-NCV-157, 160-LV-161, C206
Y58A	5R, 57-RAYG-60, 76-DLGSGSGRD-84, 101-IDMT-104, Q107, 134-GYIE-137, 155-NCV-157, 160-LV-161, C206
G60A	57-RYYA-60, 77-DLGSGSGRD-84, 101-IDMT-104, Q107, 134-GYIE-137, 155-NCV-157, 160-LV-161
L77A	57-RYYG-60, 76-DAGSGSG-82, D84, 101-IDMT-104, Q107, 134-GYIE-137, 155-NCV-157, 160-LV-161, C206
G80A	57-RYYG-60, 76-DLGSASG-82, D84, 101-IDMT-104, Q107, 134-GYIE-137, 155-NCV-157, 160-LV-161
S81A	57-RYYG-60, 76-DLGSGSGRD-84, 101-IDMT-104, Q107, 134-GYIE-137, 155-NCV-157, 160-LV-161
G82A	57-RYYG-60, 76-DLGSGSA-82, D84, 101-IDMT-104, Q107, 134-GYIE-137, 155-NCV-157, 160-LV-161
R83A	57-RYYG-60, 76-DLGSGSG-82, D84, 101-IDMT-104, Q107, 134-GYIE-137, 155-NCV-157, 160-LV-161, C206
I101A	57-RYYG-60, 76-DLGSGSG-82, D84, 101-ADMT-104, Q107, 134-GYIE-137, 155-NCV-157, 160-LV-161, C206
T104A	57-RYYG-60, 76-DLGSGSGRD-84, 101-IDMA-104, Q107, 134-GYIE-137, 155-NCV-157, 160-LV-161
G134A	57-RYYG-60, 76-DLGSGSG-82, D84, 101-IDMT-104, Q107, 134-AYIE-137, 155-NCV-157, 160-LV-161
Y135A	57-RYYG-60, 76-DLGSGSG-82, D84, 101-IDMT-104, Q107, 134-GAIE-137, 155-NCV-157, 160-LV-161, C206
N155A	57-RYYG-60, 76-DLGSGSG-82, D84, 101-IDMT-104, Q107, 134-GYIE-137, 155-ACV-157, 160-LV-161, C206
V157A	57-RYYG-60, 76-DLGSGSG-82, D84, 101-IDMT-104, Q107, 134-GYIE-137, 155-NCA-157, 160-LV-161
L160A	57-RYYG-60, 76-DLGSGSGRD-84, 101-IDMT-104, Q107, 134-GYIE-137, 155-NCV-157, 160-AV-161, C206
V161A	57-RYYG-60, 76-DLGSGSG-82, D-84, 101-IDMT-104, Q107, 134-GYIE-137, 155-NCV-157, L160

one or more nearly-invariant residues have been identified as the SAM-binding regions of the Rossmann-fold methyltransferase [21]. Four motifs of hAS3MT 76-DLGSGSG-82, 101-ID-102, 147-ESHDIVVSN-155 and 174-VLKHGGELYF-183 have been deduced as the SAM-binding regions [7,20]. The model of hAS3MT-SAM with CmArsM as template presents the residues 5.0 Å around SAM, i.e. 57-RYYG-60, 76-DLGSGSGRD-84, 101-IDMT-104, Q107, 134-GYIE-137, 155-NCV-157, 160-LV-161 and C206 [20,22]. The functions of these residues have been studied in this study and previous literature. Mutants Y59A, G60A, D76P, D76N, G78A, G80A, D84P, D84N, I101A, D102P, D102N, N155A, C156S, L160A and C206S are completely inactive. The catalytic activities of mutants R57A, Y58A, G82A, R83A, M103A, Q107A, Y135A, I136A, E137A and V161A are also obviously depressed. Residues C156 and C206 have been verified as active and As-binding sites [17]. Residues Y59, D76, G78, D84 and D102 also affect the catalytic activity of hAS3MT by affecting SAM-binding as well as residues M103, I136 and E137. As evidenced by the higher $K_{M(SAM)}$ values of mutants R57A, Y58A, G82A, R83A, Y135A and V161A than that of WT, their affinities to SAM are reduced, which further decrease their catalytic activities. Moreover, the catalytic activity of mutant S79A exceeds that of WT. Although S79 and S81 belong to the motif 76-DLGSGSG-82, they have no effects on the SAM-binding and catalytic activity of hAS3MT.

As indicated by the experiment data herein, earlier studies and the model of hAS3MT-SAM, 57-RYYG-60, 76-DLGxGxGRD-84, 101-IDMT-104, 134-GYIE-137, 155-NCV-157, 160-LV-161 and C206 are the SAM-binding sites, where x represents that the residues do not affect SAM-binding. C156 and L160 are the common residues located 5 Å around SAM and 5 Å around As atom (Fig. 7A and B) and are situated between S^+-CH_3 of SAM and As atom associated with inactive mutants C156S and L160A, indicating that they affect both SAM-binding and methyl transfer process. N155 next to the active site C156 also impacts the catalytic activity of hAS3MT. Hydrophobic residues G60, L77, G78, G80, G82, I101, M103, G134, I136, V157, L160 and V161 frame a hydrophobic environment for SAM, and acidic residues D76, D84 and D102 form hydrogen bonds with SAM directly or via water molecule. Residue Y59 has been deduced to bind SAM through cation-π and van der Waals interactions [22]. Residues R57, Y58 and G60 next to Y59 also affect SAM-binding. Adjacent Y58 and Y59 with the same side chain probably play similar roles in SAM-binding and distinguishing SAM from its analog SAH. Residues G78, G80 and G82 belonging to the consensus GxGxG are located in a loop connecting the first β-strand and α-helix in the Rossmann fold core. They are in contact with the carboxypropyl moiety of SAM. Located in the middle of β-strand 1, D76 is a highly conserved acidic residue. Conserved residue D102, which is located in the C terminus of β-strand 2, forms two hydrogen bonds with the ribose hydroxyl group of SAM. M103 and I136 with large aliphatic side chains form a sandwich structure with the nucleoside of SAM in the center. Aromatic side chain Y135 and the larger hydrophobic residue I136 stabilize the adenine moiety of SAM. 57-RYYG-60 located near methionine and residue 155-NC-156 adjacent to sulfonium S^+-CH_3 interact with methionine and S^+-

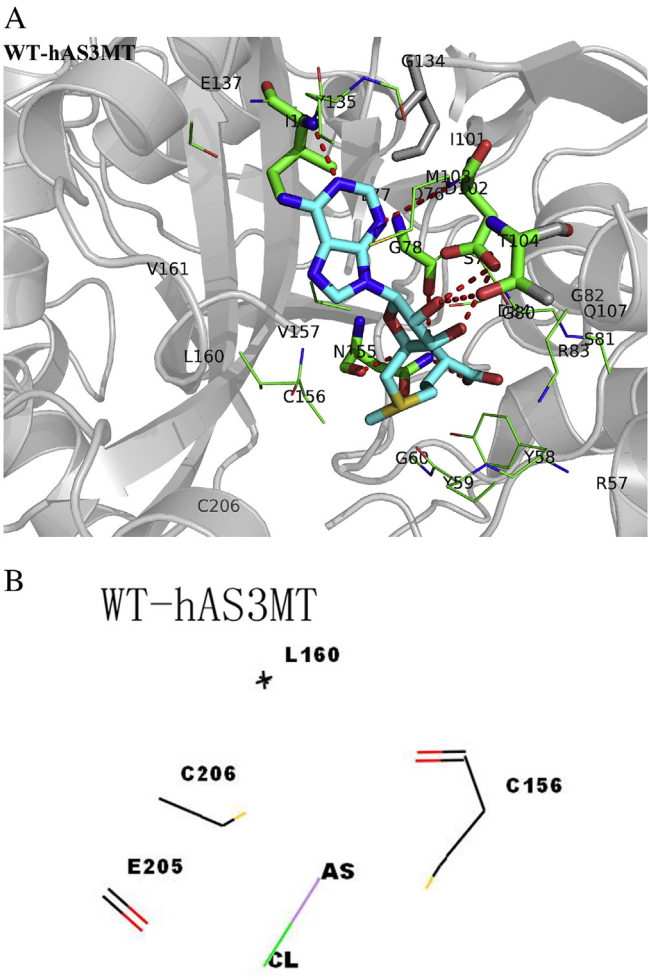

Fig. 7. Model of WT-hAS3MT with SAM and WT-hAS3MT with As. Only residues in hAS3MT ranged 5 Å around SAM and As are presented, and the hydrogen bond network formed around SAM is also marked.

CH_3 of SAM. The residues of hAS3MT, which exert effects on the breakage of C–S^+ bond in SAM, are prerequisite for catalyzing the methyl group transfer from SAM to As atom. Y59, N155, C156 and L160 that interact with S^+-CH_3 of SAM orient S^+-CH_3 during its approach to the arsenic lone pair and further activate the methyl transfer process. Furthermore, Fig. 7 displays that residues G78, D102, M103, T104, I136 and N155 form hydrogen bonds with SAM.

5. Conclusion

In summary, we designed sixteen mutants R57A, Y58A, G60A, L77A, G80A, S81A, G82A, R83A, I101A, T104A, G134A, Y135A, N155A, V157A, L160A and V161A, determined their catalytic activities, characterized their conformations and built their models. Mutants G60A, G80A, I101A, N155A and L160A were completely inactive, and the catalytic activities of other mutants were also impaired compared with that of WT. Their $K_{M(SAM)}$ values showed that the affinities to SAM were decreased. The specific functions of these residues located 5 Å around SAM were finally analyzed based on the experimental results herein, previous studies as well as the models of mutants with SAM.

Conflict of interest

The authors declared no conflict of interest.

Acknowledgments

This work is supported by the National Basic Research Program of China (2013CB922102) and the National Natural Science Foundation of China (21275072, 21201101 and 21475059).

References

[1] P. Kurttio, E. Pukkala, H. Kahelin, A. Auvinen, J. Pekkanen, Arsenic concentrations in well water and risk of bladder and kidney cancer in Finland, Environ. Health Perspect. 107 (1999) 1–6.
[2] M.F. Hughes, B.D. Beck, Y. Chen, A.S. Lewis, D.J. Thomas, Arsenic exposure and toxicology: a historical perspective, Toxicol. Sci. 123 (2011) 305–332.
[3] K. Jomova, Z. Jenisova, M. Feszterova, S. Baros, J. Liska, D. Hudecova, C.J. Rhodes, M. Valko, Arsenic: toxicity, oxidative stress and human disease, J. Appl. Toxicol. 31 (2011) 95–107.
[4] A.M. Florea, D. Büsselberg, The two opposite facets of arsenic: toxin and anticancer drug, J. Local Glob. Health Sci. 1 (2013) 1–14.
[5] X.W. Zhang, X.J. Yan, Z.R. Zhou, F.F. Yang, Z.Y. Wu, H.B. Sun, W.X. Liang, A.X. Song, V. Lallemand-Breitenbach, M. Jeanne, Q.Y. Zhang, H.Y. Yang, Q.H. Huang, G.B. Zhou, J.H. Tong, Y. Zhang, J.H. Wu, H.Y. Hu, H. Thé, S.J. Chen, Z. Chen, Arsenic trioxide controls the fate of the PML-RARa oncoprotein by directly binding PML, Science 328 (2010) 240–243.
[6] D.J. Thomas, J.X. Li, S.B. Waters, W.B. Xing, L.Y.M. Adair, Z. Drobna, V. Devesa, M. Styblo, Arsenic (+3 oxidation state) methyltransferase and the methylation of arsenicals, Exp. Biol. Med. 232 (2007) 3–13.
[7] S. Lin, Q. Shi, F.B. Nix, M. Styblo, M.A. Beck, K.M. Herbin-Davis, L.L. Hall, J.B. Simeonsson, D.J. Thomas, A novel S-adenosyl-L-methionine:arsenic(III) methyltransferase from rat liver cytosol, J. Biol. Chem. 277 (2002) 10795–10803.
[8] X.F. Ren, M. Aleshin, W.J. Jo, R. Dills, D.A. Kalman, C.D. Vulpe, M.T. Smith, L.P. Zhang, Involvement of N-6 adenine-specific DNA methyltransferase 1 (N6AMT1) in arsenic biomethylation and its role in arsenic-induced toxicity, Environ. Health Perspect. 119 (2011) 771–777.
[9] L. Ding, R.J. Saunders, Z. Drobna, F. Walton, P. Xun, D.J. Thomas, M. Styblo, Methylation of arsenic by recombinant human wild-type arsenic (+3 oxidation state) methyltransferase and its methionine 287 threonine (M287T) polymorph: role of glutathione, Toxicol. Appl. Pharm. 264 (2012) 121–130.
[10] P.K. Chiang, R.K. Gordon, J. Tal, G.C. Zeng, B.P. Doctor, K. Pardhasaradhi, P.P. McCann, S-adenosylmethionine and methylation, FASEB J. 10 (1996) 471–480.
[11] H.V. Aposhian, Enzymatic methylation of arsenic species and other new approaches to arsenic toxicity, Annu. Rev. Pharmacol. Toxicol. 37 (1997) 397–419.
[12] T. Hayakawa, Y. Kobayashi, X. Cui, S. Hirano, A new metabolic pathway of arsenite: arsenic–glutathione complexes are substrates for human arsenic methyltransferase Cyt19, Arch. Toxicol. 79 (2005) 183–191.
[13] X.L. Song, Z.R. Geng, X.L. Li, X. Hu, N.S. Bian, X.R. Zhang, Z.L. Wang, New insights into the mechanism of arsenite methylation with the recombinant human arsenic (+3) methyltransferase (hAS3MT), Biochimie 92 (2010) 1397–1406.
[14] S.P. Wang, X.L. Li, X.L. Song, Z.R. Geng, X. Hu, Z.L. Wang, Rapid-equilibrium kinetic analysis of arsenite methylation catalyzed by recombinant human arsenic (+3 oxidation state) methyltransferase (hAS3MT), J. Biol. Chem. 287 (2012) 38790–38799.
[15] D.E. Fomenko, W.B. Xing, B.M. Adair, D.J. Thomas, V.N. Gladyshev, High-throughput identification of catalytic redox-active cysteine residues, Science 315 (2007) 387–389.
[16] J.X. Li, S.B. Waters, Z. Drobna, V. Devesa, M. Styblo, D.J. Thomas, Arsenic (+3 oxidation state) methyltransferase and the inorganic arsenic methylation phenotype, Toxicol. Appl. Pharm. 204 (2005) 164–169.
[17] X.L. Song, Z.R. Geng, J.S. Zhu, C.Y. Li, X. Hu, N.S. Bian, X.R. Zhang, Z.L. Wang, Structure–function roles of four cysteine residues in the human arsenic (+3 oxidation state) methyltransferase (hAS3MT) by site-directed mutagenesis, Chem. Biol. Interact. 179 (2009) 321–328.
[18] X.L. Li, Z.R. Geng, J.Y. Chang, S.P. Wang, X.L. Song, X. Hu, Z.L. Wang, Identification of the third binding site of arsenic in human arsenic (III) methyltransferase (hAS3MT), PLoS One 8 (2013) e84231.
[19] K. Marapakala, J. Qin, B.P. Rosen, Identification of catalytic residues in the As (III) S-adenosylmethionine methyltransferase, Biochemistry 51 (2012) 944–951.
[20] X.L. Li, Z.R. Geng, S.P. Wang, X.L. Song, X. Hu, Z.L. Wang, Functional evaluation of Asp76, 84, 102 and 150 in human arsenic (III) methyltransferase (hAS3MT) interacting with S-adenosylmethionine, FEBS Lett. 587 (2013) 2232–2240.
[21] P.Z. Kozbial, A.R. Mushegian, Natural history of S-adenosylmethionine -binding proteins, BMC Struct. Biol. 5 (2005) 1–26.
[22] X.L. Li, J. Cao, S.P. Wang, Z.R. Geng, X.L. Song, X. Hu, Z.L. Wang, Residues in human arsenic (+3 oxidation state) methyltransferase forming potential hydrogen bond network around S-adenosylmethionine, PLoS One 8 (2013) e76709.
[23] T. Kuroki, T. Matsushima, Performance of short-term tests for detection of human carcinogens, Mutagenesis 2 (1987) 33–37.
[24] Z.R. Geng, X.L. Song, Z. Xing, J.L. Geng, S.C. Zhang, X.R. Zhang, Z.L. Wang, Effects of selenium on the structure and function of recombinant human S-adenosyl-L-methionine dependent arsenic (+3 oxidation state) methyltransferase in *E. coli*, J. Biol. Inorg. Chem. 14 (2009) 485–496.
[25] M.M. Bradford, A rapid and sensitive method for the quantitation of microgram quantities of protein utilizing the principle of protein-dye binding, Anal. Biochem. 72 (1976) 248–254.
[26] J. Gailer, S. Madden, W.R. Cullen, M.B. Denton, The separation of dimethylarsinic acid, methylarsonous acid, methylarsonic acid, arsenate and dimethylarsinous acid on the Hamilton PRP-X100 anion-exchange column, Appl. Organomet. Chem. 13 (1999) 837–843.
[27] G. Raber, K.A. Francesconi, K.J. Irgolic, W. Goessler, Determination of 'arsenosugars' in algae with anion-exchange chromatography and an inductively coupled plasma mass spectrometer as element-specific detector, Fresenius J. Anal. Chem. 367 (2000) 181–188.
[28] F.S. Walton, S.B. Waters, S.L. Jolley, E.L. LeCluyse, D.J. Thomas, M. Styblo, Selenium compounds modulate the activity of recombinant rat AsIII methyltransferase and the methylation of arsenite by rat and human hepatocytes, Chem. Res. Toxicol. 16 (2003) 261–265.
[29] G.L. Kedderis, A.R. Elmore, E.A. Crecelius, J.W. Yager, T.L. Goldsworthy, Kinetics of arsenic methylation by freshly isolated B6C3F1 mouse hepatocytes, Chem. Biol. Interact. 161 (2006) 139–145.
[30] W.W. Cleland, Steady state kinetics, in: P.D. Boyer (Ed.), The Enzymes, Academic Press, New York, 1970, pp. 1–65.
[31] J.T. Yang, C.S.C. Wu, H.M. Martinez, Calculation of protein conformation from circular dichroism, Methods Enzymol. 130 (1986) 208–257.
[32] S. Krimm, J. Bandekar, Vibrational spectroscopy and conformation of peptides, polypeptides and proteins, Adv. Protein Chem. 38 (1986) 181–364.
[33] W.K. Surewicz, H.H. Mantsch, New insight into protein secondary structure from resolution-enhanced infrared-spectra, Biochim. Biophys. Acta 952 (1988) 115–130.
[34] A.A. Ajees, K. Marapakala, C. Packianathan, B. Sankaran, B.P. Rosen, Structure of an As (III) S-adenosylmethionine methyltransferase: insights into the mechanism of arsenic biotransformation, Biochemistry 51 (2012) 5476–5485.
[35] P. Benkert, S.C.E. Tosatto, D. Schomburg, QMEAN: a comprehensive scoring function for model quality assessment, Proteins 71 (2008) 261–277.
[36] W.L. DeLano, The PyMOL User's Guide, DeLano Scientific LLC, San Carlos, California, USA, 2004.
[37] Y. Xu, Y. Wang, Q. Zheng, X. Li, B. Li, Y. Jin, X. Sun, G. Sun, Association of oxidative stress with arsenic methylation in chronic arsenic-exposed children and adults, Toxicol. Appl. Pharm. 232 (2008) 142–149.
[38] R.A. Copeland, Enzymes: a Practical Introduction to Structure, Mechanism, and Data Analysis, second ed., 2000.
[39] N. Sreerama, R.W. Woody, Computation and analysis of protein circular dichroism spectra, Methods Enzymol. 383 (2004) 318–351.
[40] W.C. Johnson, Analyzing protein circular dichroism spectra for accurate secondary structures, Proteins 35 (1999) 307–312.
[41] A. Dong, P. Huang, W.S. Caughey, Redox-dependent changes in β-extended chain and turn structures of cytochrome c in water solution determined by second derivative amide I infrared spectra, Biochemistry 31 (1992) 182–189.

[42] X.L. Song, Z.R. Geng, X.L. Li, Q. Zhao, X. Hu, X.R. Zhang, Z.L. Wang, Functional and structural evaluation of cysteine residues in the human arsenic (+3 oxidation state) methyltransferase (hAS3MT), Biochimie 93 (2011) 369–375.
[43] M. Fontecave, M. Atta, E. Mulliez, S-adenosylmethionine: nothing goes to waste, Trends Biochem. Sci. 29 (2004) 243–249.
[44] A.M. Wuosmaa, L.P. Hager, Methyl chloride transferase: a carbocation route for biosynthesis of halometabolites, Science 249 (1990) 160–162.
[45] V. Anantharaman, E.V. Koonin, L. Aravind, Comparative genomics and evolution of proteins involved in RNA metabolism, Nucl. Acids Res. 30 (2002) 1427–1464.
[46] D.J. Thomas, S.B. Waters, M. Styblo, Elucidating the pathway for arsenic methylation, Toxicol. Appl. Pharm. 198 (2004) 319–326.